


Editorial for the Special Issue on “Advances in Middle Infrared Laser Crystals and Its Applications”

Xiaoming Duan ^{1,*} , Renqin Dou ^{2,*}, Linjun Li ^{3,*} and Xiaotao Yang ^{4,*}

¹ National Key Laboratory of Tunable Laser Technology, Harbin Institute of Technology, Harbin 150001, China

² The Key Laboratory of Photonic Devices and Materials, Anhui Institute of Optics and Fine Mechanics, Chinese Academy of Sciences, Hefei 230001, China

³ Heilongjiang Province Key Laboratory of Laser Spectroscopy Technology and Application, Harbin University of Science and Technology, Harbin 150001, China

⁴ College of Power and Energy Engineering, Harbin Engineering University, Harbin 150001, China

* Correspondence: xmduan@hit.edu.cn (X.D.); drq0564@aiofm.ac.cn (R.D.); llj7897@126.com (L.L.); yangxiaotao@hrbeu.edu.cn (X.Y.)

In the past two decades, there has been a growing interest in middle infrared (mid-IR) laser crystals and its application to achieve mid-IR laser radiations, which has been benefited by the development of novel mid-infrared crystals and the improving quality of traditional mid-IR crystals. The recent progress in crystal growth, theoretical modelling, and generation of mid-IR laser radiations has offered a new perspective for design and growth of mid-IR crystals. In this Special Issue of *Crystals*, we gathered sixteen peer-reviewed papers that shed light on recent advances in the field of mid-IR laser crystals and their applications.

Li et al. reported the lasing performance of a Ho:YVO₄ crystal under laser diode (LD) pumping conditions [1]. With double-pass-pumped architecture, up to 8.7 W continuous-wave (CW) output power at 2052.4 nm was achieved. In addition, good beam quality factors in horizontal and vertical directions were also obtained. Yudin et al. explored the influence of angstrom-scale roughness on the laser-induced damage threshold of ZnGeP₂ crystal [2]. In the polishing process, the magnetorheological processing technology was used. Samples of the ZnGeP₂ with an Angstrom level of surface roughness were achieved. The laser-induced damage threshold value at the indicated orders of magnitude of the surface roughness parameters was determined by the number of point depressions. The influence on the characteristics of multilayer Interference antireflection coatings was also investigated, based on Nb, Si, and Al oxides on the laser-induced damage threshold of ZnGeP₂ crystal [3]. Under the excitation of a 2.09- μ m Ho:YAG laser, the effect of the defect structure and the parameters of antireflection interference coatings based on alternating layers of Nb₂O₅/Al₂O₃ and Nb₂O₅/SiO₂ layers on the laser-induced damage threshold of ZnGeP₂ crystals were determined. Experimental results indicate that the silicon conglomerates in an interference antireflection coating is beneficial to decrease the laser-induced damage threshold of the ZnGeP₂ crystal. Li et al. prepared the β -Ga₂O₃ saturable absorber by the optical floating zone method [4], which was used in subsequent work, the 1.08- μ m Nd:GYAP laser produces 606.54-ns pulse width at repetition rate of 344.06 kHz. Experimental results present that the β -Ga₂O₃ crystal has great potential for the development of the 1- μ m pulsed laser. Liao et al. explored the energy transfer and cross-relaxation induced 2.78 μ m emission in Er³⁺/Tm³⁺: PbF₂ crystal [5], which was grown by the Bridgman method. The spectroscopic properties, energy transfer mechanism, and first-principles calculations of as-grown crystals were investigated in detail. This work provides an avenue to design mid-IR laser materials with good performance. Wang et al. investigated the characteristics of plasma generated by infrared pulse laser-induced fused silica [6]. Based on the theory of fluid mechanics and gas dynamics, a two-dimensional axisymmetric gas dynamic model was established to simulate the plasma generation process



Citation: Duan, X.; Dou, R.; Li, L.; Yang, X. Editorial for the Special Issue on “Advances in Middle Infrared Laser Crystals and Its Applications”. *Crystals* **2022**, *12*, 643. <https://doi.org/10.3390/cryst12050643>

Received: 25 April 2022

Accepted: 26 April 2022

Published: 30 April 2022

Publisher’s Note: MDPI stays neutral with regard to jurisdictional claims in published maps and institutional affiliations.



Copyright: © 2022 by the authors. Licensee MDPI, Basel, Switzerland. This article is an open access article distributed under the terms and conditions of the Creative Commons Attribution (CC BY) license (<https://creativecommons.org/licenses/by/4.0/>).

of fused silica induced by a millisecond pulse laser. The maximum expansion velocity of the laser-induced plasma was calculated. The experimental results verify the correctness of theoretical calculations. Kim et al. theoretically and numerically investigated the broad-band second-harmonic properties of non-oxide mid-IR nonlinear crystals [7]. Chalcopyrite semiconductors, defect chalcopyrite and orthorhombic ternary chalcogenides have also been demonstrated. Beam propagation directions, spectral positions of resonance, effective nonlinearities, spatial walk-offs between interacting beams and spectral bandwidths were analyzed. Zheng et al. investigated the mid-IR optical property of Dy:CaF₂-SrF₂ crystal [8], which was fabricated by a multicrucible temperature gradient method. Sellmeier dispersion formula, absorption characteristics and fluorescence properties were demonstrated. The results indicate that the Dy:CaF₂-SrF₂ crystal is a promising candidate for compact mid-IR lasers. Chen et al. show the internal mechanism of APD photocurrent characteristics under ms-level pulsed infrared laser irradiation [9]. The sampling current characteristics of the external circuit and the internal mechanism of the current generation in APD were studied. Chen et al. also investigated the temperature-rise characteristics of silicon avalanche photodiodes in different external capacitance circuits irradiated by the same laser pulse [10]. Zhang et al. explored the formation laws of direction of Fano line-shape in a ring MIM plasmonic waveguide side-coupled with a rectangular resonator and nano-sensing analysis of multiple fano resonances [11]. Du et al. presented an experimental investigation of double-end pumped Tm, Ho:GdVO₄ laser [12]. With operating temperature of 77 K, the output characteristics of Tm, Ho:GdVO₄ laser were studied, where the continuous-wave and Q-switching performance were also demonstrated. Ni et al. investigated the mid-far properties of nonlinear crystal AGGSe [13]. The large AGGSe single crystal of 35 mm diameter and 80 mm length was obtained by the seed-aided Bridgman method. X-ray diffraction, rocking curve and transmission spectrum was used to characterize the crystalline quality. In addition, the 8 μm frequency doubling was also presented. Qian et al. reported a high energy, narrow pulse width, long-wave infrared ZGP optical parametric oscillator [14]. The maximum average output powers of 3.15 W at 8.2 μm and 11.4 W at 2.8 μm were achieved. The minimum pulse width was approximately 8.1 ns. Niu et al. reported an efficient pulsed Ho:YAP laser pumped at 1989 nm [15]. When the absorbed power was 30 W, an average power of 18.02 W with the pulse width of 104.2 ns acousto-optic (AO) Q-switched Ho:YAP laser was obtained at a repetition frequency of 10 kHz. Ma et al. experimentally investigated the plasma plume analysis of long pulse laser irradiates CFRP and GFRP composite materials [16]. The results show that GFRP is more vulnerable to breakdown than CFRP under the same conditions.

As shown in this Special Issue of *Crystals*, the study of mid-IR crystals and its applications continues to grow and expand as we, as a community, strive to acquire further understanding of the underlying potential of these crystals. The goal is to bring these and other new concepts closer to application for mid-IR crystals and beyond.

Funding: This research received no external funding.

Conflicts of Interest: The authors declare no conflict of interest.

References

1. Li, Y.; Zhang, C.; Ji, Q. Efficient Ho:YVO₄ Laser Double-Pass-Pumped by a Wavelength-Stabilized Laser Diode. *Crystals* **2022**, *12*, 320. [[CrossRef](#)]
2. Yudin, N.; Khudoley, A.; Zinoviev, M.; Podzvalov, S.; Slyunko, E.; Zhuravleva, E.; Kulesh, M.; Gorodkin, G.; Kumeysya, P.; Antipov, O. The Influence of Angstrom-Scale Roughness on the Laser-Induced Damage Threshold of Single-Crystal ZnGeP₂. *Crystals* **2022**, *12*, 83. [[CrossRef](#)]
3. Yudin, N.N.; Zinoviev, M.; Gladkiy, V.; Moskvichev, E.; Kinyaevsky, I.; Podzyvalov, S.; Slyunko, E.; Zhuravleva, E.; Pfaf, A.; Yudin, N.A.; et al. Influence of the Characteristics of Multilayer Interference Antireflection Coatings Based on Nb, Si, and Al Oxides on the Laser-Induced Damage Threshold of ZnGeP₂ Single Crystal. *Crystals* **2021**, *11*, 1549. [[CrossRef](#)]
4. Li, B.; Chen, Q.; Zhang, P.; Tian, R.; Zhang, L.; Sai, Q.; Wang, B.; Pan, M.; Liu, Y.; Xia, C.; et al. β-Ga₂O₃ Used as a Saturable Sbsorber to Realize Passively Q-Switched Laser Output. *Crystals* **2021**, *11*, 1501. [[CrossRef](#)]

5. Liao, J.; Chen, Q.; Niu, X.; Zhang, P.; Tan, H.; Ma, F.; Li, Z.; Zhu, S.; Hang, Y.; Yang, Q.; et al. Energy Transfer and Cross-Relaxation Induced Efficient 2.78 μm Emission in $\text{Er}^{3+}/\text{Tm}^{3+}:\text{PbF}_2$ mid-Infrared Laser Crystal. *Crystals* **2021**, *11*, 1024. [[CrossRef](#)]
6. Wang, L.; Sun, X.; Geng, C.; Zhang, Z.; Cai, J. A Study of the Characteristics of Plasma Generated by Infrared Pulse Laser-Induced Fused Silica. *Crystals* **2021**, *11*, 1009. [[CrossRef](#)]
7. Kim, I.; Lee, D.; Lee, K.J. Investigation of Mid-Infrared Broadband Second-Harmonic Generation in Non-Oxide Nonlinear Optic Crystals. *Crystals* **2021**, *11*, 921. [[CrossRef](#)]
8. Zheng, L.; Zhao, J.; Wang, Y.; Chen, W.; Ruan, F.; Lin, H.; Xue, Y.; Liu, J.; Liu, Y.; Yang, R.; et al. Mid-IR Optical Property of $\text{Dy}:\text{CaF}_2\text{-SrF}_2$ Crystal Fabricated by Multicrucible Temperature Gradient Technology. *Crystals* **2021**, *11*, 907. [[CrossRef](#)]
9. Chen, L.; Wang, D.; Jin, G.-Y.; Wei, Z. Study on the Internal Mechanism of APD Photocurrent Characteristics Caused by the ms Pulsed Infrared Laser Irradiation. *Crystals* **2021**, *11*, 884. [[CrossRef](#)]
10. Chen, L.; Wei, Z.; Wang, D.; Liu, H.-X.; Jin, G.-Y. Temperature Rise Characteristics of Silicon Avalanche Photodiodes in Different External Capacitance Circuits Irradiated by Infrared Millisecond Pulse Laser. *Crystals* **2021**, *11*, 866. [[CrossRef](#)]
11. Zhang, D.; Cheng, L.; Shen, Z. Formation Laws of Direction of Fano Line-Shape in a Ring MIM Plasmonic Waveguide Side-Coupled with a Rectangular Resonator and Nano-Sensing Analysis of Multiple Fano Resonances. *Crystals* **2021**, *11*, 819. [[CrossRef](#)]
12. Du, Y.; Dai, T.; Sun, H.; Kang, H.; Xia, H.; Tian, J.; Chen, X.; Yao, B. Experimental Investigation of Double-End Pumped Tm, Ho: GdVO_4 Laser at Cryogenic Temperature. *Crystals* **2021**, *11*, 798. [[CrossRef](#)]
13. Ni, Y.; Hu, Q.; Wu, H.; Han, W.; Yu, X.; Mao, M. The Investigation on Mid-Far Infrared Nonlinear Crystal $\text{AgGaGe}_5\text{Se}_{12}$ (AGGSe). *Crystals* **2021**, *11*, 661. [[CrossRef](#)]
14. Qian, C.; Yu, T.; Liu, J.; Jiang, Y.; Wang, S.; Shi, X.; Ye, X.; Chen, W. A High-Energy, Narrow-Pulse-Width, Long-Wave Infrared Laser Based on ZGP Crystal. *Crystals* **2021**, *11*, 656. [[CrossRef](#)]
15. Niu, C.; Jiang, Y.; Wen, Y.; Zhao, L.; Chen, X.; Wu, C.; Dai, T. High-Efficiency Ho:YAP Pulse Laser Pumped at 1989 nm. *Crystals* **2021**, *11*, 595. [[CrossRef](#)]
16. Ma, Y.; Xin, C.; Zhang, W.; Jin, G. Experimental Study of Plasma Plume Analysis of Long Pulse Laser Irradiates CFRP and GFRP Composite Materials. *Crystals* **2021**, *11*, 545. [[CrossRef](#)]